Computer Assisted Methods in Engineering and Science
33(2): 85–99, 2026, https://doi.org/10.24423/cames.2026.1786

Algorithm for Processing Broadband Dielectric Spectroscopy Data of Heterogeneous Materials

Alexander Tonkoshkur[1)], Andrey Shcherbak[1)], Alexander Lyashkov[2)*]

[1)] *Department of Electronic Computing Machinery, Oles Honchar Dnipro National University, Dnipro, Ukraine*
[2)] *Department of Applied Radiophysics, Electronics and Nanomaterials, Oles Honchar Dnipro National University, Dnipro, Ukraine*

[*] *Corresponding Author: alexdnu@ukr.net*

This work focuses on the development of computational techniques for processing dielectric measurement data, particularly those from broadband dielectric spectroscopy. A novel approach is formulated and tested for software implementation, enabling the selection of parameter sets for known dispersion models used in analyzing complex dielectric spectra of heterogeneous materials.
The proposed algorithm divides the wide frequency range of measurements into shorter subranges corresponding to distinct observed dispersion regions. These regions are identified using one (or more known phenomenological relaxation models via least-squares methods (LSMs), deconvolution, and other techniques.
Testing of the algorithm on the frequency-dependent complex dielectric permittivity of varistor ceramic materials demonstrated satisfactory accuracy and physical consistency of the results. These findings highlight the efficiency and potential of the proposed approach.

Keywords: dielectric spectroscopy, data processing, algorithm, complex spectrum, ZnO ceramics.

1. Introduction

In materials science, dielectric spectroscopy has long been a fundamental investigative tool for understanding the electrical and chemical structure, as well as the physical properties, of heterogeneous substances and objects [1, 2]. This method is extensively used in the development and application of various heterogeneous electronic materials (ceramics, glasses, composites) [3–5], the synthesis of new materials based on organic polymers [6–8], and the study of biological and medical objects [9–11].

Modern measurement systems allow for highly accurate investigation of the dielectric properties of various physical media across a wide range of frequencies and temperatures. Fully automated spectrometers have two significant implications [12]:

– the need to handle vast amounts of data,

– the ability to model using sums of relaxation functions.

In broadband dielectric spectroscopy, the complex dielectric permittivity (CDP) is determined at specific measurement frequencies. As the spectra are discrete datasets, only numerical approximations can be used. The accuracy of the selected mathematical methods significantly influences the assessment of the models' suitability [13]. Therefore, the processing and analysis of experimental data remain pressing tasks to this day.

The development of universal algorithms and software for processing and analyzing dielectric measurement data is typically based on well-known models of frequency dispersion of dielectric permittivity, such as the Debye formula or its phenomenological generalizations, including the Cole–Cole, Davidson–Cole, and Havriliak–Negami models [1, 14–16].

A key feature of these models is their versatility, which allows for multipurpose applications, including:

– analytical representation of experimental data for more accurate descriptions,

– interpretation of the parameters of these relationships and their dependencies on various factors, based on specific physical models of polarization processes in various materials and objects,

– derivation of information about general parameters of heterogeneity in dielectric relaxation processes, such as the distribution of relaxation times and the shape of this distribution.

The methodology for processing and analysis based on generalized models using sums of relaxation functions, rooted in the additivity of polarization processes, represents a significant advancement in the dielectric spectroscopy method [1, 2, 17, 18]. Nevertheless, the individual characteristics of the relaxation processes in different materials and objects remain a significant factor hindering the development of universal algorithms and the implementation of computer technologies in this area. A potential solution may involve grouping materials and objects with similar polarization process sets and developing algorithms and software templates tailored to these groups.

It should be noted that the most well-known mathematical procedure for selecting a model of dielectric relaxation processes is the least-squares method (LSM), which enables the determination of all model parameters [19–21]. However, for complex spectra, this entails minimizing a multi-variable function,

which is a sum of several relaxation functions. Each relaxation function may involve two (Debye model) to four (Havriliak–Negami model) adjustable parameters and may not be unimodal. Additional challenges arise when processing overlapping dispersion regions.

To address the complexities of processing and analyzing intricate dielectric spectra, a decomposition-based approach shows potential:

- dividing the initial wide-frequency experimental spectrum into shorter subranges where dispersion dependencies are present. These dependencies might be represented as declining (low-frequency dispersion regions) or ascending (high-frequency dispersion regions) functions, which may not be fully captured in the available data;
- sequentially processing these shorter spectrum segments, beginning with the extremes and considering their impact on adjacent dispersion regions;
- utilizing theoretical insights into relaxation processes in the material or object to guide the selection of these frequency subranges and initial approximations for the parameters of the chosen approximating models.

This approach enables the application of the LSM for analyzing each specific frequency segment, the use of deconvolution procedures to determine relaxation times in overlapping dispersion regions [22–24], and the application of Kramers–Kronig relations to account for through-conductivity (via direct current), among other established methods [25–30].

In this study, we explore the application of this approach to the development of an algorithm for processing and analyzing dielectric spectra of heterogeneous materials. For validation, dielectric spectra of high-voltage varistor zinc oxide (ZnO) ceramics were utilized as experimental data over a broad frequency range.

2. Broadband dielectric spectrum model and data processing algorithm

Based on established concepts of the linear additive nature of contributions from individual dielectric relaxation processes to a complex broadband spectrum [1, 2, 17, 18], the model expression for the entire frequency range can be represented as a sum of corresponding elementary models. Within the approach discussed here – dividing the initial wide frequency range of the dielectric spectrum into shorter subranges – the generalized model for the frequency dispersion of the CDP over the entire range can be expressed as:

$$\epsilon^*\left(f, M\right) = \epsilon_h + \sum_{i=1}^{R}\sum_{j=1}^{N_i}\left[\epsilon^*_{i,j}\left(f, M_i^{\langle j\rangle}\right) - \epsilon_{i.j}^{(h)}\right], \tag{1}$$

where R is the number of subranges; N_i is the number of elementary models in the i-th subrange; $\epsilon^*_{i,j}\left(f, M_i^{\langle j\rangle}\right)$ and $\epsilon^{(h)}_{i.j}$ are the j-th elementary model for the frequency dispersion of CDP in the ith subrange and its high-frequency (post-dispersion) value for the real part, respectively; i ($i = 1, ..., R$) and j ($j = 1, ..., N_i$) are its indices; f is the frequency; $M_i^{\langle j\rangle}$ is the set of parameters for the elementary model (including the relaxation time $\tau_{i,j}$, the difference $\Delta_{i,j} = \epsilon^{(l)}_{i.j} - \epsilon^{(h)}_{i.j}$, where $\epsilon^{(h)}_{i.j}$ is the high-frequency value and $\epsilon^{(l)}_{i.j}$ is the low-frequency value of the real part of the CDP and other parameters. Thus, $M_i^{\langle j\rangle} = \{\tau_{i,j}, \Delta_{i,j}, \alpha_{i,j}, \beta_{i,j}$ (where, depending on the selected mode, the parameters α and / or β may be absent); M is the set of parameters for the generalized model; ϵ_h is the high-frequency value of the real part of the CDP for the highest-frequency dispersion region.

The mathematical implementation of the considered approach for computer processing and preliminary analysis of dielectric spectra can be represented by the following algorithm:

1. Determination of clearly distinguishable separate dispersion regions in the initial experimental frequency dependence of the imaginary part of the CDP, i.e., identification of R frequency subranges between the minima of the dielectric loss coefficient ε''.
2. Selection of models and determination of initial approximate parameter values for the extreme left and right subranges ($i = 1$ and $i = R$) directly from the processed experimental dependencies.

   In particular, using the experimental values of the maximum of the imaginary part of the CDP $\varepsilon''(f_{\max})$, for the considered subrange and the corresponding frequency $f_{\max}$, it is possible to estimate the initial approximate values of the relaxation time $\tau^{(0)} = 1/(2\pi \cdot f_{\max_1})$ and the absolute magnitude of the dispersion amplitude of the real part of the CDP $\Delta^{(0)} =\geq 2 \cdot \varepsilon''(f_{\max_1})$ (the indices of the dispersion region i and j are omitted for simplicity).

   It should be noted that in some cases an appropriate value for $\Delta^{(0)}$ can also be directly determined from the experimental frequency dependence of the real part of the CDP as $\Delta^{(0)} = \varepsilon_{l0} - \varepsilon_{h0}$, where ε_{l0} and ε_{h0} are the low-frequency (static) and high-frequency values of the real part of the CDP, respectively.

   In the case of broadened (overlapping) dispersion regions, it is advisable to apply deconvolution methods [22–24] to separate them and determine the initial values of the dielectric relaxation times. If complete data on a dispersion region are not available, it is permissible to use prior values for the model parameters based on known literature data and

physical concepts of the relaxation process under consideration. The remaining parameters are chosen arbitrarily within the range of permissible values.

3. Approximation of the extreme left ($i = 1$) and right ($i = R-1$) dispersion regions of the selected models using the LSM and determination of more accurate parameter values for the models, which ensure the minimal absolute error of the LSM target functions [31] in these ranges, is performed as follows:

$$\Phi_i\left(f_k, M_i^{\langle 1\rangle}, M_i^{\langle 2\rangle}, ..., M_i^{\langle N_i\rangle}\right) = \sum_{k=1}^{K_i}\left\{\log\varepsilon_k'' - \log\left[\sum_{j=1}^{N_i}\epsilon_{i,j}''\left(f_k, M_i^{\langle j\rangle}\right)\right]\right\}^2 \to \min, \quad (2)$$

where $\epsilon_{i,j}''\left(f_k, M_i^{\langle j\rangle}\right) = -\mathrm{Im}\left[\epsilon_{i,j}^*\left(f_k, M_i^{\langle j\rangle}\right)\right]$; K_i is the number of experimental points in the i-th subrange ($i = 1$ or R). The value $N_i \neq 1$ in cases of overlapping dispersion regions in a single subrange and when the deconvolution procedure is applied for their separation.

4. Correction of the experimental dependencies $\varepsilon_k''(f)$ for internal subranges ($i = 2, 3, ..., R-1$) is performed by subtracting from them the corresponding calculated values of the imaginary part of the CDP, obtained by extrapolating analytical expressions of models already identified in previously processed dispersion regions:

$$\overline{\varepsilon}_k''\big|_{i=2...N-1} = \varepsilon_k'' - \left[\sum_{j=1}^{N_1}\epsilon_{i,j}''\left(f_k, M_i^{\langle j\rangle}\right) + \sum_{j=1}^{N_R}\epsilon_{i,j}''\left(f_k, M_i^{\langle j\rangle}\right)\right]. \quad (3)$$

5. Sequential repetition of the operations described in the previous two steps using the corrected data allows determination of the parameter values of the selected models for internal subranges (i.e., approximation of the extreme left and right subranges $i = 2$ and $i = R-2$, followed by $i = 3$ and $i = R-3$, and so on).

6. Final refinement of the parameters of the generalized additive model (1) for the entire range of the initial experimental broadband dielectric spectrum with K points is performed by minimizing the LSM target function as follows:

$$\Phi\left(f_k, M\right) = \sum_{k=1}^{K}\left\{\log\varepsilon_k'' - \log\left[\epsilon''\left(f_k, M\right)\right]\right\}^2,$$

where $\epsilon''\left(f, M\right) = -\mathrm{Im}\left\{\epsilon^*\left(f, M\right)\right\}$.

7. Error assessment of the approximation for the frequency dependencies of the real and imaginary parts of the CDP can be performed using the ratio of the root-mean-square deviation to the mean value of the experimental dependency (the coefficient of variation of the approximation):

$$v^{(x)} = \sqrt{\left\{\sum_{k=1}^{K}\left[\varepsilon_k^{(x)} - \epsilon^{(x)}\left(f_k, M\right)\right]^2 \Big/ (K-1)\right\}} \Big/ \sum_{k=1}^{K} \varepsilon_k^{(x)}/K, \qquad (4)$$

where (x) corresponds to 'double prime' $(\prime\prime)$ for the imaginary part and 'prime' $(\prime)$ for the real part of the CDP, and $\epsilon'(f) = \mathrm{Re}\left\{\epsilon^*\left(f, M\right)\right\}$.

3. Processing of broadband dielectric spectroscopy data for ZnO-based semiconductor ceramics

This section examines the implementation of the formulated approach for processing the complex broadband dielectric spectrum of a heterogeneous semiconductor material – varistor ZnO-based ceramics – as a demonstration of its applicability.

This material's structure is characterized by a dielectric interlayer [32, 33]. In the frequency dependencies of the real ε' and imaginary ε'' parts of the CDP, several dispersion regions are observed, typical for heterogeneous systems of this type [34–37]:

- a maximum (or decrease), at low and infralow frequencies $f < 10^2$ Hz region (I), associated with the capture of electrons from ZnO crystallites into their 'slow' surface electronic states;
- a broadened maximum ε'' at intermediate frequencies (10^4 to 10^6 Hz), interpreted as the superposition of two relaxation processes: hopping of weakly bound charged particles (electrons) in the intracrystalline phase (II) and recharging of bulk trap levels in ZnO crystallites (III).
- high-frequency behavior: a decrease in ε' and an increase in ε'' in the range $f > 10^7$ Hz region (IV), caused by Maxwell–Wagner separation of free charges in ZnO crystallites.

The frequency dependence of $\varepsilon''(f)$ is shown in Fig. 1.

As seen in Fig. 1, the entire frequency range of the experimental dielectric spectrum can be divided into three subranges: low and infralow frequencies (dispersion region I), intermediate frequencies (regions II and III), and high frequencies (region IV). The procedure for applying the formulated algorithm to each of these subranges is presented subsequent.

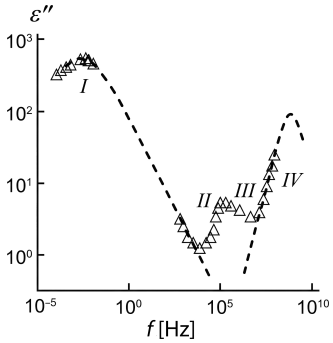

FIG. 1. Experimental frequency dependencies of the imaginary part of the CDP of ZnO-based ceramics (triangles) and the results of approximation for its low- and high-frequency regions using the Cole–Cole and Debye models (dashed lines).

3.1. SUBRANGE OF LOW AND INFRALOW FREQUENCIES

When determining a model for the relatively broad dispersion region *1*, its association with the recharging of surface electronic states, which exhibit significant statistical variability in physical parameters, must be considered. The Cole–Cole model is chosen as the most appropriate to describe the entire range (case – $N_1 = 1$) of region *1*. In the previously established notation, it has the following form:

$$\epsilon^*_{1,1}\left(f, M_1^{\langle 1\rangle}\right) = \epsilon^{(h)}_{1.1} + \frac{\Delta_{1,1}}{1 + (j2\pi f\tau_{1,1})^{\alpha_{1,1}}}, \tag{5}$$

where $M_1^1 = [\Delta_{1,1}, \tau_{1,1}, \alpha_{1,1}]$ are its parameters.

The initial approximations for the parameters of formula (5) were chosen using the maximum value of the experimental frequency dependence of the imaginary part of the CDP $\cdot\, \varepsilon''(f_{\max_1})$ and its corresponding frequency $f_{\max_1}$: $\tau^{(0)}_{1,1} = 1/(2\pi f_{\max_1})$ and $\Delta^{(0)}_{1,1} \geq 2\varepsilon''(f_{\max_1})$, and also accepted $\alpha^{(0)}_{1,1} = 0.5$.

The identification of model (5) for the data of subrange 1 was carried out using the LSM with expression (2). The sequential simplex method (SSM), one of the simplest yet effective optimization techniques, was employed to find the minimum [38–40].

The procedure for implementing the SSM consisted of the following steps:

1. Determination of target function values (2) for $(m+1)$ vertices of a convex figure (simplex) in m-dimensional space (in this case, $m = 3$) is performed by calculating the coordinates (model parameters) of the vertices using the following formula:

$$x_{ij} = x_{0j} + X_{ij} \cdot \Delta x_j, \tag{6}$$

where x_{0j} and Δx_j are the initial value and the variation step of the j-th variable in the natural coordinate system, $i = 1, ..., m$; $j = 1, ..., m+1$; X_{ij} is the coded value of the j-th variable for the i-th vertex, calculated as:

$$\geq X_{ij} = \begin{cases} -\left[\dfrac{1}{2j(j+1)}\right]^{1/2}, & i < j+1, \\ \left[\dfrac{j}{2j(j+1)}\right]^{1/2}, & i = j+1, \\ 0, & i \geq j+1. \end{cases}$$

2. Sequential exclusion of the simplex vertex with the worst target function value, replacing it with a new (reflected) vertex with coordinates:

$$x_{kj}^{(\mathrm{ref})} = \frac{2}{n}\sum_{l}^{n+1} x_{ij} - \left(\frac{2}{n}+1\right)\cdot x_{ij}^{(\mathrm{excl})}. \tag{7}$$

As a result, a new simplex is obtained, where the excluded vertex is replaced by a new vertex obtained by reflecting the excluded vertex relative to the opposite face of the initial simplex. The worst vertex is replaced in the same manner. If the vertex with the minimum target function value remains unchanged, any vertex of the last simplex is selected as the center of the plan, and the variation step is reduced. This process is repeated until the step becomes smaller than the permissible error for determining the coordinates.

The initial approximations and refined parameter values of the model are provided in Table 1, and the visual results of model identification are shown in Fig. 1.

Table 1. Parameters of models approximating the experimental dielectric spectrum.

Subrange	Dispersion region in Fig. 1		Initial approximations of model parameters			Clarified values		
	Number	Model	$\tau^{(0)}$, c	$\Delta^{(0)}$	$\alpha^{(0)}$	τ, c	Δ	α
1	*I*	Cole–Cole	$1.1\cdot10^{3}$	$1.65\cdot10^{3}$	0.5	77.2	$2.53\cdot10^{3}$	0.49
2	*II*	Cole–Cole	$8.4\cdot10^{-6}$	10.1	0.05	$8.04\cdot10^{-7}$	9.85	0.017
2	*III*	Cole–Cole	$1.5\cdot10^{-6}$	8.1	0.05	$8.41\cdot10^{-8}$	4.59	0.029
3	*IV*	Debye	$1\cdot10^{-9}$	$1.84\cdot10^{2}$	–	$2.40\cdot10^{-10}$	$1.84\cdot10^{2}$	–

3.2. High-frequency subrange

The high-frequency rise in the dependence $\varepsilon''(f)$, observed in subrange *3*, corresponds to the initial segment of dielectric dispersion caused by Maxwell

relaxation of free charges in conductive inclusions within a dielectric matrix [35]. This process typically exhibits a narrow distribution in relaxation times and can be described using the Debye model

$$\epsilon^*_{3,1}\left(f, M_3^{\langle 1\rangle}\right) = \epsilon^{(h)}_{3,1} + \frac{\Delta_{3,1}}{1 + j2\pi f\tau_{3,1}}, \tag{8}$$

where $M^{(3)} = [\Delta_{3,1}, \tau_{3,1}]$.

Given the lack of complete experimental data for this dispersion region, it is advisable to rely on physical concepts and literature data about this relaxation process when selecting initial approximations for the parameters in expression (8). This corresponds to the highest-frequency region ($f_{\max_4} \sim 10^9$ and above [35, 37, 41]), and an initial approximation for the relaxation time can be estimated as $\tau^{(0)}_{3,1} = 1/(2\pi f_{\max_4})$. The post-dispersion real part of the CDP $\epsilon^{(h)}_{i.j} = \epsilon_h$ can be estimated as the relative dielectric permittivity of the material with a heterogeneous structure and a larger volume fraction of ZnO ($\varepsilon\prime \approx 10$) [35, 42].

It should be noted that the parameter $\Delta^{(0)}_{3,1}$ can be directly determined using the formula $\Delta^{(0)}_{3,1} = \epsilon^{(l)}_{i.j} - \epsilon^{(h)}_{i.j}$, where $\epsilon^{(l)}_{i.j}$ is the pre-dispersion value of the relative dielectric permittivity, which can be derived directly from the experimental dependence of the real part of the CDP.

The identification of model (8) for the experimental data of subrange 3 was carried out in a similar manner to that described for subrange *1*, using the previously described SSM procedure (see Table 1 and Fig. 1).

3.3. Subrange of intermediate frequencies

When processing the data for the dispersion region in the intermediate frequency subrange, where an asymmetric broadened maximum of the imaginary part of the CDP is observed, the experimental spectral dependence $\varepsilon''(f)$ must first be corrected according to expression (3). Considering the broadened shape of this maximum and the physical concept of two relaxation processes present in this frequency range, the initial values of the relaxation times were determined using the deconvolution method described in [22].

To apply this method, the corrected experimental dependence in the intermediate frequency subrange was represented analytically as $\overline{\varepsilon}''(r)$, where $r = \log(f_0/f)$ and $f_0 = 1\,\text{Hz}$ is a constant reference frequency. The Cole–Cole formula was used as the model for dielectric dispersion in the corresponding regions.

In this case, the distribution function of relaxation times $G(\tau)$ as a function of the generalized coordinate $s = \log(\tau/\tau_0)$, where $\tau_0 = 1/(2\pi f_0)$ is an arbitrary value, has the form:

$$G(s) = \int_{-\infty}^{\infty} \epsilon''(r) T''(s-r) \mathrm{d}r. \tag{9}$$

Here, the function $T''(r)$ is defined as

$$T''(r) = \frac{16k}{\pi} \int_0^{\infty} \widetilde{W}(p) \cosh\left(\frac{\pi^2 p}{k}\right) \cos(2\pi p r)\, \mathrm{d}r,$$

which is derived in [22] based on the general expression for the CDP in terms of a convolution equation with the relaxation time distribution function and its solution via direct (denoted by a tilde) and inverse Fourier transforms, using the Kaiser–Bessel digital filtering window:

$$\widetilde{W}(p) = \begin{cases} \dfrac{I_0\left[\pi a \sqrt{1-(p/p_m)^2}\right]}{I_0[\pi a]}, & |p| \le p_m, \\ 0, & |p| > p_m, \end{cases}$$

where $I_0(x) = \sum_{k=0}^{\infty} \left[\frac{(x/2)^k}{k!}\right]^2$ is the modified Bessel function of the first kind and of order zero.

For the analysis, the recommended window parameters were used: $p_m = 3$ (window width parameter) and $\pi a = 2$ (a is a non-negative real number determining the window shape) [43].

Figure 2 presents the results of applying the described deconvolution procedure to the experimental frequency dependence of the imaginary part of the CDP in the intermediate frequency subrange shown in Fig. 1.

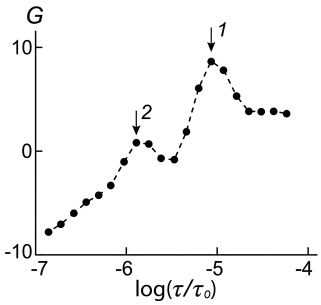

Fig. 2. Relaxation time distribution function obtained for the experimental frequency dependence of the imaginary part of the CDP (Fig. 1) in the intermediate frequency subrange. The identified peaks correspond to dispersion regions *II* (*1*) and *III* (*3*) in Fig. 1.

As seen in Fig. 2, the dependence can be associated with two relaxation processes characterized by relaxation times $\tau_{2,1}^{(0)}$ and $\tau_{2,2}^{(0)}$, which are subsequently

used as their initial values (Table 1). The parameters $\Delta_{2,1}^{(0)}$ and $\Delta_{2,2}^{(0)}$ are estimated using the earlier expression $\tau\Delta_{i,j}^{(0)} \sim 2 \cdot \overline{\varepsilon}''|_{f=1/2\pi_{i,j}^{(0)}}$.

The additional parameters $\alpha_{2,1}^{(0)}$ and $\alpha_{2,2}^{(0)}$ for the Cole–Cole model are chosen arbitrarily (using trial methods aimed at improving calculation efficiency).

Refinement of the parameters of the selected approximation models for the identified dispersion regions is performed by fitting the models to the experimental data using the LSM, which involves minimizing the target function given by expression (2). The results obtained are shown in Fig. 3 and Table 1.

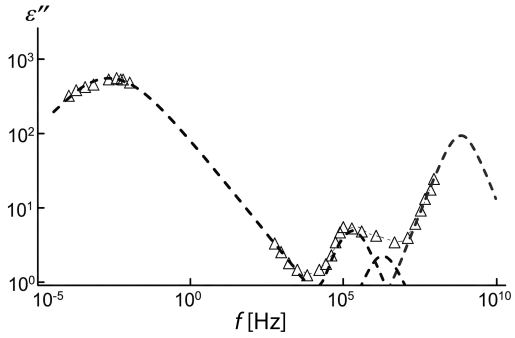

Fig. 3. Experimental frequency dependence of the imaginary part of the CDP of ZnO-based varistor ceramics (triangles) and approximations of its individual dispersion regions using selected phenomenological models (dashed lines).

3.4. Model parameters for the entire frequency range

Based on the analysis conducted, the experimental frequency dependence of the imaginary part of the CDP over the entire investigated range can be described by four relaxation processes. The appropriate analytical mathematical model (1) consists of the sum of three dispersion expressions corresponding to the Cole–Cole model and one Debye formula.

It should be noted that further refinement of the parameters of this additive model for the entire range of the experimental dielectric spectrum, following the general algorithm described earlier (Sec. 2), provided estimates of all its parameters. These values differed only slightly from those obtained earlier when processing each relaxation process individually in its respective frequency subrange. The refined values are presented in Table 1.

The results of applying this processing and preliminary analysis method to several experimental dielectric spectra of ZnO-based varistor ceramics are shown in Fig. 4.

The approximation error estimates for the frequency dependencies of the real and imaginary parts of the CDP, based on formula (4), yielded values $v \leq 10\,\%$.

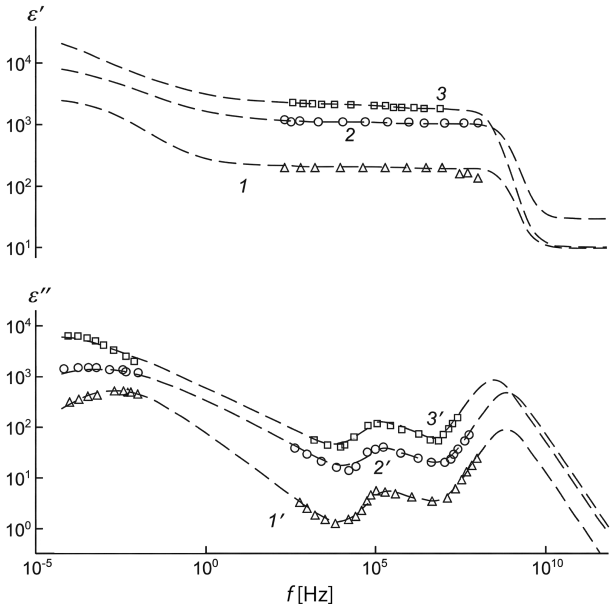

Fig. 4. Frequency dependencies of the real ε' and imaginary ε'' parts of the CDP of ZnO-based varistor ceramics, fabricated at synthesis temperatures T_C, K: *1*, *1′* – 1173; *2*, *2′* – 1423; *3*, *3′* – 1573 (symbols of different shapes), and the results of approximation using the generalized additive model for the entire investigated range (dashed lines).

4. Conclusions

An algorithm for processing and analyzing complex dielectric spectra over a wide frequency range has been proposed. The algorithm includes:

- dividing the entire frequency range into several shorter subranges corresponding to separate observable dispersion regions;
- identifying each of these subranges into the experimental spectrum using one of the well-known elementary phenomenological relaxation models, sequentially, starting from the extreme dispersion regions and accounting for their influence on adjacent internal regions;
- refining the parameters of the generalized additive model, which represents the sum of elementary models for the selected subranges, using the complete experimental broadband dielectric spectrum and the LSM.

The developed algorithm was tested by processing the frequency dependencies of the CDP of ZnO-based varistor ceramic materials. The results showed satisfactory agreement with existing physical concepts and demonstrated the efficiency and potential of this approach for developing computer technologies for processing and preliminary analysis of experimental dielectric spectra of a wide range of heterogeneous materials.

References

1. Kremer F., Schönhals A. [Eds], *Broadband Dielectric Spectroscopy*, Springer Science & Business Media, 2002.
2. Poplavko Y., *Dielectric Spectroscopy of Electronic Materials: Applied Physics of Dielectrics*, Woodhead Publishing, 2021.
3. Elbashar Y.H. *et al.*, Electric, dielectric and optical properties of doped metal oxide glasses: A review, *Nonlinear Optics, Quantum Optics: Concepts in Modern Optics*, **52**(1–2): 1–36, 2020.
4. Yang H., Zhang S., Yang H., Li E., Usage of P–V–L bond theory in studying the structural/property regulation of microwave dielectric ceramics: A review, *Inorganic Chemistry Frontiers*, **7**(23): 4711–4753, 2020, https://doi.org/10.1039/D0QI00907E.
5. Shanmugasundram H.P.P.V., Jayamani E., Soon K.H., A comprehensive review on dielectric composites: Classification of dielectric composites, *Renewable and Sustainable Energy Reviews*, **157**: 112075, 2022, https://doi.org/10.1016/j.rser.2022.112075.
6. Popov I., Cheng S., Sokolov A.P., Broadband dielectric spectroscopy and its application in polymeric materials, [in:] *Macromolecular Engineering: From Precise Synthesis to Macroscopic Materials and Applications*, Hadjichristidis N., Gnanou Y., Matyjaszewski K. *et al.* [Eds], Wiley, pp. 1–39, 2022, https://doi.org/10.1002/9783527815562.mme0059.
7. Teyssedre G., Zheng F., Boudou L., Laurent C., Charge trap spectroscopy in polymer dielectrics: A critical review, *Journal of Physics D: Applied Physics*, **54**(26): 263001, 2021, https://doi.org/10.1088/1361-6463/abf44a.
8. Kumbhakar K., Pham T.D., Lee K.K., Kwak K., Cho M., Dielectric relaxation spectroscopy for the characterization of ion transport in solid polymer electrolytes in Li-ion cells, *Electrochimica Acta*, **462**: 142759, 2023, https://doi.org/10.1016/j.electacta.2023.142759.
9. Fahmy H.M. *et al.*, Dielectric spectroscopy signature for cancer diagnosis: A review, *Microwave and Optical Technology Letters*, **62**(12): 3739–3753, 2020, https://doi.org/10.1002/mop.32517.
10. Schreiner T.G., Adam M., Broadband dielectric spectroscopy and its role in the characterization of biological cells, *Bulletin of the Polytechnic Institute of Iaşi. Electrical Engineering, Power Engineering, Electronics Section*, **67**(1): 9–20, 2021, https://doi.org/10.2478/bipie-2021-0001.
11. Mertens M., Chavoshi M., Peytral-Rieu O., Grenier K., Schreurs D., Dielectric spectroscopy: Revealing the true colors of biological matter, *IEEE Microwave Magazine*, **24**(4): 49–62, 2023, https://doi.org/10.1109/MMM.2022.3233510.
12. Wübbenhorst M., van Turnhout J., Analysis of complex dielectric spectra. I. One-dimensional derivative techniques and three-dimensional modelling, *Journal of Non-Crystalline Solids*, **305**(1–3): 40–49, 2002, https://doi.org/10.1016/S0022-3093(02)01086-4.
13. Haspel H., Kukovecz Á., Kónya Z., Kiricsi I., Numerical differentiation methods for the logarithmic derivative technique used in dielectric spectroscopy, *Processing and Application of Ceramics*, **4**(2): 87–93, 2010, https://doi.org/10.2298/PAC1002087H.
14. Koposov G.D., Volkov A.S., Tyagunin A.V., Perfiliev R.O., Numerical simulation method for identification of experimental results according to frequency dispersion of dielectric permittivity by Gavrylyak-Negami, [in:] *IOP Conference Series: Earth and Environmental Science*, **263**(1): 012059, 2019, https://doi.org/10.1088/1755-1315/263/1/012059.

15. Rosa C.F.A.E., Capelas de Oliveira E., Relaxation equations: Fractional models, *Journal of Physical Mathematics*, **6**(2): 1–7, 2015, https://doi.org/10.4172/2090-0902.1000146.

16. Barelli E., *Dielectric Relaxation in Biological Materials*, Master Thesis, Scuola di Scienze Corso di Laurea in Fisica, Universita di Bologna, 2015, https://amslaurea.unibo.it/9102/1/Eleonora_Barelli_tesi.pdf.

17. Odinaev S., Makhmadbegov R.S., Frequency dispersion of dielectric permittivity and dielectric losses in aqueous KCl and CsCl solutions depending on their state parameters, *Ukrainian Journal of Physics*, **60**(12): 1211–1211, 2015, https://doi.org/10.15407/ujpe60.12.1211.

18. Moon Y.I., Jung J.K., Chung K.S., Dielectric relaxation spectroscopy in synthetic rubber polymers: Nitrile butadiene rubber and ethylene propylene diene monomer, *Advances in Materials Science and Engineering*, **1**: 8406059, 2020, https://doi.org/10.1155/2020/8406059.

19. Bello A., Laredo E., Grimau M., Comparison of analysis of dielectric spectra of PCL in the ε^* and the M^* formalism, *Journal of Non-Crystalline Solids*, **353**(47–51): 4283-4287, 2007, https://doi.org/10.1016/j.jnoncrysol.2007.08.041.

20. Boukamp B.A., Distribution (function) of relaxation times, successor to complex nonlinear least squares analysis of electrochemical impedance spectroscopy?, *Journal of Physics: Energy*, **2**(4): 042001, 2020, https://doi.org/10.1088/2515-7655/aba9e0.

21. Sabnis S.M., Rander D.N., Kanse K.S., Joshi Y.S., Kumbharkhane A.C., Spectroscopic measurement and dielectric relaxation study of vegetable oils, *Information Processing in Agriculture*, **11**(3): 397–408, 2024, https://doi.org/10.1016/j.inpa.2023.04.002.

22. Salefran J.L., Dutuit Y., The use of a discriminative window in deconvolution method applied to dielectric data, *The Journal of Chemical Physics*, **74**(5): 3056–3063, 1981, https://doi.org/10.1063/1.441430.

23. Nicholson D.J., Kell D.B., Davey C.L., Deconvolution of the dielectric spectra of microbial cell suspensions using multivariate calibration and artificial neural networks, *Bioelectrochemistry and Bioenergetics*, **39**(2): 185–193, 1996, https://doi.org/10.1016/0302-4598(95)01890-5.

24. Ganea C.P., Zgura I., Frunza L., Numerical deconvolution approaches for dielectric characteristics of complex composite materials based on liquid crystals and oxide nanopowders, *Materials Chemistry and Physics*, **309**: 128372, 2023, https://doi.org/10.1016/j.matchemphys.2023.128372.

25. Steeman P.A.M., van Turnhout J., Fine structure in the parameters of dielectric and viscoelastic relaxations, *Macromolecules*, **27**(19): 5421–5427, 1994, https://doi.org/10.1021/ma00097a023.

26. van Turnhout J., Wübbenhorst M., Analysis of complex dielectric spectra. II: Evaluation of the activation energy landscape by differential sampling, *Journal of Non-Crystalline Solids*, **305**(1–3): 50–58, 2002, https://doi.org/10.1016/S0022-3093(02)01120-1.

27. Schäfer H., Sternin E., Stannarius R., Arndt M., Kremer F., Novel approach to the analysis of broadband dielectric spectra, *Physical Review Letters*, **76**(12): 2177, 1996, https://doi.org/10.1103/PhysRevLett.76.2177.

28. van Turnhout J., Better resolved dielectric dispersions by the apt use of Kramers–Kronig relations, differential operators, and all-in-1 modeling, [in:] *Current Topics on Chemistry and Biochemistry*, Vol. 5, pp. 40–82, 2022, https://doi.org/10.9734/bpi/ctcb/v5/3055C.

29. Güneşer M.T., Artificial intelligence solution to extract the dielectric properties of materials at sub-THz frequencies, *IET Science, Measurement & Technology*, **13**(4): 523–528, 2019, https://doi.org/10.1049/iet-smt.2018.5356.

30. Saadaoui Y., Zegnini B., Seghier T., Analysis of dielectric relaxation spectra by diffusive representations method: Case of organic dielectrics, *Przeglad Elektrotechniczny*, **97**(8): 52–58, 2021, https://doi.org/10.15199/48.2021.08.10.

31. Shoup T.E., *A Practical Guide to Computer Methods for Engineers*, Prentice-Hall, Englewood Cliffs, New York, 1979.

32. Gupta T.K., Application of zinc oxide varistors, *Journal of the American Ceramic Society*, **73**(7): 1817–1840, 1990, https://doi.org/10.1111/j.1151-2916.1990.tb05232.x.

33. Ganesh K.S., A review of zinc oxide varistors for surge arrester, [in:] *2018 4th International Conference on Electrical Energy Systems (ICEES)*, pp. 470–474, 2018.

34. Tonkoshkur A.S., Glot A.B., Ivanchenko A.V., Basic models in dielectric spectroscopy of heterogeneous materials with semiconductor inclusions, *Multidiscipline Modeling in Materials and Structures*, **13**(1): 36–57, 2017, https://doi.org/10.1108/MMMS-08-2016-0037.

35. Tonkoshkur A.S., Effect of charge exchange of local centers on dielectric phenomena in disperse semiconductor structures, *Ukrainskii Fizicheskii Zhurnal*, **23**: 2030–2038, 1978.

36. Avdeenko B.K., Tonkoshkur A.S., Chernenko I.M., Dielectric losses in oxide-zinc ceramics, *Inorganic Materials*, **18**: 1028, 1982.

37. Fernandez-Hevia D., Peiteado M., de Frutos J., Caballero A.C., Fernandez J.F., Wide range dielectric spectroscopy of ZnO-based varistors as a function of sintering time, *Journal of the European Ceramic Society*, **24**(6): 1205–1208, 2004, https://doi.org/10.1016/S0955-2219(03)00411-4.

38. Corriou J.P., *Numerical Methods of Optimization. Theory and Practice for Engineers*, Springer International Publishing, 2021.

39. Michałowska-Kaczmarczyk A.M., Michałowski T., Simplex optimization and its applicability for solving analytical problems, *Journal of Applied Mathematics and Physics*, **2**(7): 723–736, 2014, https://doi.org/10.4236/jamp.2014.27080.

40. Cerdà V., Cerdà J.L., Idris A.M., Optimization using the gradient and simplex methods, *Talanta*, **148**: 641–648, 2016, https://doi.org/10.1016/j.talanta.2015.05.061.

41. Levinson L.M., Philipp H.R., High-frequency and high-current studies of metal oxide varistors, *Journal of Applied Physics*, **47**(7): 3116–3121, 1976, https://doi.org/10.1063/1.323059.

42. Samsonov G.V., *Physicochemical Properties of Oxides* [in Russian], Metallurgy, Moscow, 1976.

43. Nuttall A., Some windows with very good sidelobe behavior, *IEEE Transactions on Acoustics, Speech, and Signal Processing*, **29**(1): 84–91, 1981, https://doi.org/10.1109/TASSP.1981.1163506.

Received January 7, 2025; revised February 25, 2026; accepted March 3, 2026; available online March 10, 2026; version of record April 20, 2026; published issue June 17, 2026.